Kinetic simulation model of magnetron discharges

I. A. Porokhova,[1] Yu. B. Golubovskii,[2] J. Bretagne,[3] M. Tichy,[4] and J. F. Behnke[1]
[1]*Ernst-Moritz-Arndt-University Greifswald, Domstrasse 10A, 17487 Greifswald, Germany*
[2]*St. Petersburg State University, St. Petergof, Ulianovskaia 1, 198904 St. Petersburg, Russia*
[3]*Laboratoire de Physique des Gaz et Plasmas, Bâtiment. 210, Universite Paris–Sud, 91405 Orsay Cedex, France*
[4]*Charles University in Prague, V Holesovickach 2, 180 00 Prague, Czech Republic*
(Received 13 July 2000; published 26 April 2001)

A self-consistent kinetic model of plasma in the entire gap of a magnetron cylindrical discharge, with all quantities varying in radius and with the uniform magnetic field being directed axially, is presented. The discharge modeling is performed on the basis of a numerical solution of the spatially inhomogeneous Boltzmann kinetic equation together with equations of ion motion, current balance, and Poisson's equation. The model represents an example of discharge description from cathode to anode with respect to strong nonlocality effects in the distribution function formation. Based on the results for a typical magnetron discharge condition, the distribution functions, field, and macroscopic properties calculated for the entire discharge in argon, are presented and discussed.

DOI: 10.1103/PhysRevE.63.056408 PACS number(s): 52.25.Dg, 51.10.+y, 52.40.Hf

INTRODUCTION

The cylindrical magnetron discharge widely used in technological applications to create and etch thin films, represents a discharge between two coaxial electrodes (inner cathode and outer anode) at pressures of hundredths of Torr and currents of about 100 mA. This discharge in a radial electric field E, can be sustained in the presence of axially directed magnetic field B of the strength of hundreds Gauss. Modeling of the magnetron dc discharge may yield a deeper understanding of both the fundamental issues in gas discharge physics and of the practical aspects of cylindrical magnetron control.

Unlike cylindrical unmagnetized or magnetized discharges where the radial electric field of ambipolar diffusion is orthogonal to the axial field of current transport, in cylindrical magnetrons these fields are both directed radially. At magnetic field strengths employed in the experiments, the Larmor radius of electron cyclotron motion $r_{ec}=v/\omega_{eB}$ ($\omega_{eB}=eB/m$ is the electron cyclotron frequency, v is the velocity, and e and m are the elementary charge and electron mass) becomes smaller than the distance between cathode and anode. Electrons are magnetized, whereas a magnetic field has no substantial influence on ion motion. For this reason, electron and ion current densities contributing to discharge current appear to be comparable to each other.

The modeling of inhomogeneous plasma at low pressures and small currents, where nonlocal effects are of major importance, has been successfully developed recently. The effects of nonlocal formation of the electron distribution function (EDF) in the positive column are investigated particularly in examples of classical cylindrical discharges in Refs. [1–4]. For investigations of cathode phenomena without a magnetic field, where nonlocal formation of the strongly anisotropic EDF and ionization rate becomes especially apparent, the particle simulation methods [5–7] or Monte Carlo simulation [8–12], analytical methods taking into consideration continuous energy loss approximations [13,14], or hybrid hydrodynamic models [15,16], and a recently developed multiterm method for solving the kinetic equation [17], are used. Nonlocal phenomena caused by a disturbing action of the anode on the EDF have been interpreted in Refs. [18,19].

Kinetic modeling of magnetron configuration discharge, based on a strict solution to the nonlocal Boltzmann kinetic equation, is very effective for the following reasons. First, the presence of an axial magnetic field remarkably reduces the anisotropy of the distribution function in the radial direction. This circumstance considerably simplifies the procedure for kinetic equation solution in the cathode region, since in this case no use of Monte Carlo or multiterm techniques is required. Thus it becomes possible to obtain a quite reliable solution of the kinetic equation by the two-term approximation for the entire discharge gap between cathode and anode. Second, the condition that the discharge current density and the ambipolar current density are directed radially results in the reduction of the problem to one dimension in the real space. This is of particular importance when describing electron and ion fluxes in the near-electrode regions, where axial and radial fluxes are strongly redistributed due to ionizing collisions. Finally, kinetic modeling permits us to describe the discharge gap in more detail than is usually achieved by particle simulation methods.

This paper represents an attempt at self-consistent kinetic modeling of magnetron discharge plasma in crossed electric and magnetic fields. The electron component of plasma is analyzed on the basis of a numerical solution of spatially dependent Boltzmann kinetic equations supplemented by a hydrodynamic description of ions and by Poisson's equation for field distribution. A similar theory permits us to obtain self-consistently the profiles of electric field and macroscopic parameters from cathode to anode. A kinetic treatment appears to be more efficient than the particle simulation techniques, as it permits us to consider in detail the electron distribution function formation in the cathode sheath and negative glow regions, trace its transition from the positive column towards equipotential anode, and analyze the processes of electron relaxation in the cathode-fall sheath. Par-

ticular calculations are performed for discharge in argon under the conditions specified in Ref. [5].

ELECTRON KINETICS

The electron component will be analyzed starting with the spatially inhomogeneous Boltzmann equation for the electrons with charge $-e$ and mass m

$$\vec{v}\cdot\nabla_{\vec{r}}F-\frac{e}{m}(\vec{E}+[\vec{v}\times\vec{B}])\cdot\nabla_{\vec{v}}F=C(F). \tag{1}$$

The electron distribution function $F(\vec{v},\vec{r})$ is formed under the influence of spatial gradients, the action of radial electric and axial magnetic fields, and various collision processes $[C(F)]$. When using a two-term expansion of the distribution function in spherical harmonics, the EDF can be represented in the form

$$\begin{aligned}F(\vec{v},\vec{r})&=F_0(v)+\vec{F}_1\cdot\frac{\vec{v}}{v}\\&=F_0(v)+\frac{v_r}{v}F_{1r}(v)+\frac{v_\theta}{v}F_{1\theta}(v)+\frac{v_z}{v}F_{1z}(v),\end{aligned} \tag{2}$$

where $F_0(v)$ is the isotropic distribution and $F_{1r}(v)$, $F_{1\theta}(v)$, and $F_{1z}(v)$ are the radial, azimuth, and axial components of the vector EDF anisotropy.

Substitution of expansion (2) into the kinetic equation (1) after integration over solid angles yields

$$\frac{1}{3}\nabla_{\vec{r}}\cdot\vec{F}_1-\frac{e}{m}\frac{1}{v^2}\frac{\partial}{\partial v}(v^2\vec{E}\cdot\vec{F}_1)=C_0,$$

$$v\nabla_{\vec{r}}F_0-\frac{e\vec{E}}{m}\frac{\partial F_0}{\partial v}-\frac{e}{m}[\vec{B}\times\vec{F}_1]=\vec{C}_1.$$

Taking into account that $\vec{E}=E(r)\vec{k}_r$, $\vec{B}=B\vec{k}_z$, and $\vec{C}_1=-(v/\lambda_e)\vec{F}_1$ (λ_e is electron free path), we obtain the following expressions for the anisotropic components:

$$f_{1r}(U,r)=\frac{\lambda_e}{1+(\lambda_e/r_{ec})^2}\left[-\frac{\partial f_0}{\partial r}+eE(r)\frac{\partial f_0}{\partial U}\right], \tag{3}$$

$$\begin{aligned}f_{1\theta}(U,r)&=\frac{r_{ec}}{1+(\lambda_e/r_{ec})^2}\left[-\frac{\partial f_0}{\partial r}+eE(r)\frac{\partial f_0}{\partial U}\right]\\&=\frac{\lambda_e}{r_{ec}}f_{1r}(U,r),\end{aligned}$$

$$f_{1z}(U,r)=0,$$

which differ from the correspondent distribution functions F by the factor $2\pi(2/m)^{3/2}$ and have the kinetic energy $U=mv^2/2$.

The kinetic equation for the isotropic distribution function can be represented as follows:

$$\frac{U}{3}\frac{1}{r}\frac{\partial}{\partial r}rf_{1r}(U,r)-\frac{eE(r)}{3}\frac{\partial}{\partial U}Uf_{1r}(U,r)=S_0(f_0), \tag{4}$$

where the collision operator

$$S_0(f_0)=S_0^{\mathrm{el}}(f_0)+S_0^{\mathrm{ex}}(f_0)+S_0^{\mathrm{di}}(f_0)+S_0^{\mathrm{si}}(f_0)$$

includes elastic and inelastic collisions and direct and stepwise ionization collisions:

$$S_0^{\mathrm{el}}(f_0)=2\frac{m}{M}\frac{\partial}{\partial U}[U^2NQ^{\mathrm{el}}(U)f_0(U,r)],$$

$$\begin{aligned}S_0^{\mathrm{ex}}(f_0)=&-UNQ^{\mathrm{ex}}(U)f_0(U,r)\\&+(U+U_{\mathrm{ex}})NQ^{\mathrm{ex}}(U+U_{\mathrm{ex}})f_0(U+U_{\mathrm{ex}},r),\end{aligned}$$

$$\begin{aligned}S_0^{\mathrm{di}}(f_0)=&-UNQ^{\mathrm{di}}(U)f_0(U,r)\\&+(U/\beta+U_{\mathrm{di}})NQ^{\mathrm{di}}(U/\beta+U_{\mathrm{di}})\\&\times f_0(U/\beta+U_{\mathrm{di}},r)/\beta\\&+[U/(1-\beta)+U_{\mathrm{di}}]NQ^{\mathrm{di}}[U/(1-\beta)+U_{\mathrm{di}}]\\&\times f_0[U/(1-\beta)+U_{\mathrm{di}},r]/(1-\beta)\end{aligned}$$

$$\begin{aligned}S_0^{\mathrm{si}}(f_0)=&-UN_mQ^{\mathrm{si}}(U)f_0(U,r)\\&+(U/\beta+U_{\mathrm{si}})N_mQ^{\mathrm{si}}(U/\beta+U_{\mathrm{si}})\\&\times f_0(U/\beta+U_{\mathrm{si}},r)/\beta\\&+[U/(1-\beta)+U_{\mathrm{si}}]N_mQ^{\mathrm{si}}[U/(1-\beta)+U_{\mathrm{si}}]\\&\times f_0[U/(1-\beta)+U_{\mathrm{si}},r]/(1-\beta).\end{aligned}$$

Here $Q^{\mathrm{el}}(U)$ and $Q^{\mathrm{ex}}(U)$ denote the total cross sections for momentum transfer and excitation collisions with the excitation threshold of U_{ex}, $Q^{\mathrm{di}}(U)$ and $Q^{\mathrm{si}}(U)$ are the cross sections of direct and stepwise ionization with the corresponding ionization potentials U_{di} and U_{si}, M is the atom mass, N is the density of gas atoms, which is related to gas pressure p in Torr by $N=pN_g$, where $N_g=3.54\times10^{16}$ cm^{-3}, and N_m is the density of the metastable atoms involved in stepwise ionization processes. The density N_m was taken equal to 10^{11} cm^{-3}. These cross sections are represented in Fig. 1. The ionization operators are written under the assumption that after each ionization event the remaining kinetic energy U of the colliding electron is shared between the two outgoing electrons with the ratio βU and $(1-\beta)U$ $(0<\beta<1)$.

An important influence on electron kinetics produced by the magnetic field consists in the abrupt reduction of the radial anisotropy f_{1r} and the appearance of the azimuth component $f_{1\theta}$, which was zero in the absence of a magnetic field. It is seen from Eq. (3) that the anisotropic distribution function f_{1r} for magnetized electrons ($r_{ec}\ll\lambda_e$) is smaller by the factor $(r_{ec}/\lambda_e)^2$ than the corresponding anisotropic part of the EDF formed in a discharge without a magnetic field. Even under conditions of weak magnetic fields and low pres-

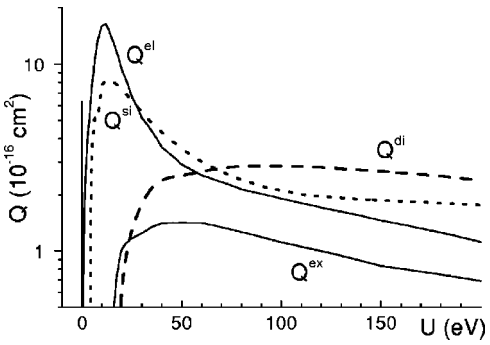

FIG. 1. Total cross sections of elastic and inelastic collisions, and of direct and stepwise ionization for argon, used in the calculations.

sures, the inequality $r_{ec}/\lambda_e<1$ valid for the energies $U<m\omega_{eB}^2/\{2[NQ_\Sigma(U)]\}$, holds well for electron energies of several hundreds eV. The azimuth anisotropy is larger than the radial one by the factor of ratio λ_e/r_{ec} and might be dominant in the expansion (2). In this connection the two-term expansion (2) becomes sufficient to obtain an appropriate description of the EDF formation in the cathode sheath at not too low pressures and not too small magnetic field strengths.

The system (3), (4) can be simplified by changing variables from U to the total energy $\varepsilon=U+e\varphi(r)$, with radial potential energy $e\varphi(r)=-\int_{R_a}^{r}E(r)dr(-e)$, yielding

$$\frac{1}{3}U\frac{1}{r}\frac{\partial}{\partial r}rf_{1r}(\varepsilon,r)=S_0[f_0(\varepsilon,r)], \tag{5}$$

$$f_{1r}(\varepsilon,r)=-\frac{UNQ_\Sigma}{U(NQ_\Sigma)^2+m\omega_{eB}^2/2}\frac{\partial f_0(\varepsilon,r)}{\partial r}. \tag{6}$$

Here Q_Σ denotes the total cross section of electron-atom collisions $Q_\Sigma(U)=Q^{\mathrm{el}}+Q^{\mathrm{ex}}+Q^{\mathrm{di}}+Q^{\mathrm{si}}$.

Substituting the function f_{1r} into Eq. (5), we come to the final partial differential parabolic equation for the isotropic distribution function

$$\frac{1}{r}\frac{\partial}{\partial r}\left(rA(\varepsilon,r)\frac{\partial f_0(\varepsilon,r)}{\partial r}\right)+\frac{\partial}{\partial\varepsilon}[B(\varepsilon,r)f_0(\varepsilon,r)] =C(\varepsilon,r)f_0(\varepsilon,r)-D[f_0(\varepsilon,r)] \tag{7}$$

with the coefficients

$$A(\varepsilon,r)=\frac{1}{3}\frac{U^2NQ_\Sigma}{U(NQ_\Sigma)^2+m\omega_{eB}^2/2},$$

$$B(\varepsilon,r)=2\frac{m}{M}U^2NQ_\Sigma(U),$$

where the kinetic energy is $U(\varepsilon,r)=\varepsilon-e\varphi(r)$. The excitation and ionization processes at the energy ε are described by collision integrals C and D, which can be easily obtained from the above expressions for S_0^{ex}, S_0^{di}, and S_0^{si}. In total

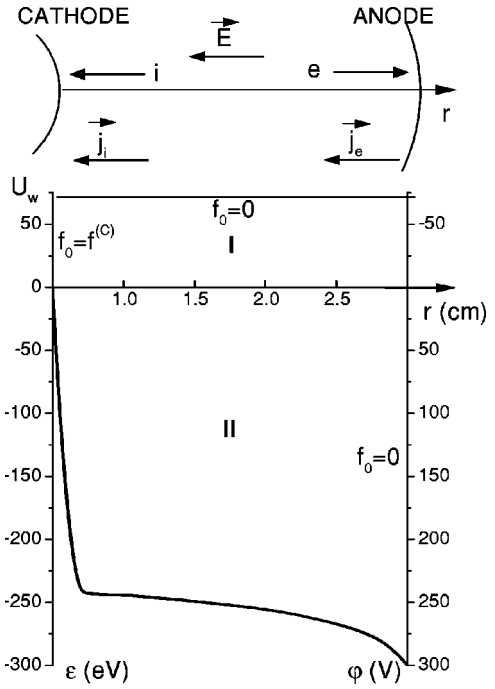

FIG. 2. Schematic representation of the discharge gap in the radial direction (top) and the solution region in variables total energy and radius (bottom). Bold curve corresponds to the potential profile obtained as a result of the self-consistent solution.

energy-coordinate space the energy ε is attained in the ionization event by those electrons whose energies before ionizing collision were $\varepsilon+U(1-\beta)/\beta+U_{\mathrm{di}}$ and $\varepsilon+U\beta/(1-\beta)+U_{\mathrm{di}}$.

The solution region of Eq. (7) is represented in Fig. 2. It is bounded above by the line $\varepsilon\leqslant U_\infty$, the left boundary corresponds to the curve where the kinetic energy is zero equal, and the right boundary is the anode. The positive direction of the r axis is taken in the direction from cathode to anode and the electric field is assumed to be negative in the whole region. The total energy is thus positive ($\varepsilon>0$) in region I and negative ($\varepsilon<0$) in region II. Due to its parabolic nature, Eq. (7) can be solved as a boundary value problem with evolution coordinate ε. The solution process must evolve from higher energies towards lower ones, to yield at every energy ε the EDF as a function of radius. More details on the numerical scheme are given in the Appendix.

Since the electrons are injected into the discharge gap from the cathode, and the problem to be solved is the boundary value problem, we can assume a definite initial distribution of electrons to be given at the cathode, and

$$f_0(\varepsilon,R_c)=f_0^{(C)}(U,R_c).$$

The PIC simulation of magnetron discharge [5] showed that the distribution function formed very near to the cathode has a continuous energy spectrum and monotonically decreases up to energies exceeding 100 eV. Thus, the distribution which is sufficiently extended towards a large energy range can be taken as being the initial distribution at the cathode.

The upper boundary of the solution region is taken from the condition that the function $f_0^{(C)}$ vanishes at $U \geqslant U_\infty$ or has negligibly small values

$$f_0(\varepsilon,r)|_{\varepsilon \leqslant U_\infty}=0.$$

The anode is an absorbing surface for the electrons which leave the discharge gap upon attaining the anode. The simplest boundary condition at the anode is the equality of the EDF to zero,

$$f_0(\varepsilon,R_a)=0,$$

which corresponds to the absence of electrons at the anode surface. A more precise boundary condition at the anode can be imposed following the Milne [20] problem on radiation escape from a dispersing medium as done in Ref. [19].

In region II the boundary condition at the curve $\varepsilon=e\varphi(r)$ $(U=0)$ can be obtained considering the kinetic equation (4) in the vicinity of vanishing kinetic energy, which reads

$$-\frac{1}{3}eE(r)f_{1r}(U,r)=S_0[f_0(U,r)]. \tag{8}$$

In a magnetic field the anisotropic component f_{1r}, according to Eqs. (3), (6) at $U\to 0$ becomes

$$f_{1r}(U,r)=-\frac{UNQ_\Sigma(0)}{m\omega_{eB}^2/2}\frac{\partial f_0}{\partial r}+eE(r)\frac{UNQ_\Sigma(0)}{m\omega_{eB}^2/2}\frac{\partial f_0}{\partial U}.$$

In small ranges of kinetic energies slightly exceeding excitation potential or ionization energy, the excitation and ionization cross sections may be approximated by linear dependence of the form $Q^a=Q_0^a(U/U_a-1)$, where index a corresponds to ex, di, or si. Substituting these linear approximations into the operator for backscattered electrons, we obtain

$$\begin{aligned}S_0[f_0(\varepsilon,r)]|_{U\to 0}=U\{&NQ_0^{\rm ex}f_0(\varepsilon+U_{\rm ex},r)\\&+[NQ_0^{\rm di}f_0(\varepsilon+U_{\rm di},r)\\&+N_mQ_0^{\rm si}f_0(\varepsilon+U_{\rm si},r)]\\&\times[1/\beta^2+1/(1-\beta)^2]\}.\end{aligned}$$

Finally, the boundary condition at the curve $\varepsilon=e\varphi(r)$ gets the following representation:

$$\begin{aligned}\left.\frac{\partial f_0(\varepsilon,r)}{\partial r}\right|_{\varepsilon=e\varphi(r)}&=\frac{3}{2}\frac{m\omega_{eB}^2}{eE(r)}\left[\frac{Q_0^{\rm ex}}{Q_\Sigma(0)}f_0(\varepsilon+U_{\rm ex},r)\right.\\&\left.+\frac{Q_0^{\rm di}}{Q_\Sigma(0)}f_0(\varepsilon+U_{\rm di},r)[1/\beta^2+1/(1-\beta)^2]\right].\end{aligned}$$

Here we neglected stepwise ionization due to the small size of the ratio N_m/N. When the magnetic field strength is zero, this condition is transformed into zero boundary condition for the derivative $\partial f_0/\partial r$ which is commonly used in similar problems.

Macroscopic radial behavior of electrons is described by the radial distributions of electron particle and current density, ionization rates, and electron average energy. These parameters can be easily obtained in terms of electron distribution function. The density and average energy of electrons are correspondingly as follows:

$$n_e(r)=\int_0^\infty f_0(U,r)U^{1/2}dU,$$

$$U_e(r)=\int_0^\infty f_0(U,r)U^{3/2}dU/n_e(r).$$

Direct and stepwise ionization rates are

$$I_d(r)=\left(\frac{2}{m}\right)^{1/2}\int_{U_{\rm di}}^\infty NQ^{\rm di}(U)f_0(U,r)UdU,$$

$$I_s(r)=\left(\frac{2}{m}\right)^{1/2}\int_{U_{\rm si}}^\infty N_mQ^{\rm si}(U)f_0(U,r)UdU,$$

and the electron current density in the radial direction is

$$j_e(r)=-\frac{1}{3}\left(\frac{2}{m}\right)^{1/2}\times\int_{e\varphi(r)}^\infty\frac{U^2NQ_\Sigma(U)}{U(NQ_\Sigma)^2+m\omega_{eB}^2/2}\frac{\partial f_0(\varepsilon,r)}{\partial r}d\varepsilon. \tag{9}$$

These macroscopic properties were calculated simultaneously while solving the kinetic equation in a way similar to that described in Ref. [1].

An appropriate averaging of the kinetic equation (5) over kinetic energies yields the following particle balance of the electrons:

$$\frac{1}{r}\frac{d}{dr}rj_e(r)=I_d(r)+I_s(r)$$

and energy balance

$$\frac{1}{r}\frac{d}{dr}rj_{eU}(r)=-eE(r)j_e(r)-H^{\rm el}-H^{\rm ex}-H^{\rm io},$$

where

$$j_{eU}(r)=\frac{1}{3}\left(\frac{2}{m}\right)^{1/2}\int_0^\infty f_{1r}(U,r)U^2dU$$

is the energy current density, $H^{\rm el}$, $H^{\rm ex}$, and $H^{\rm io}$ are the energy losses in elastic, inelastic, and ionization collisions. The form of the particle balance reflects the appearance of electrons in ionizing collisions resulting in an increase in the electron current density with magnetron discharge radius. The particle and energy balances follow identically from the

kinetic equation and are used to check the accuracy of the solution obtained for the distribution function.

ION KINETICS

To develop the self-consistent theory of magnetron discharge plasma it is necessary to combine the description of electron component with that of ion kinetics. Whereas the ion free path $\lambda_i \approx 0.25$ cm is small compared to the magnetron radius, the ions move in the collision regime and can be treated in the hydrodynamic approximation.

Ion motion, therefore, is described by the particle and force balances, where ion collisions dominate over inertia, pressure gradient, and Lorentz force term

$$\nabla \cdot n_i \vec{u}_i = I_d + I_s, \tag{10}$$

$$\vec{j}_i = n_i \vec{u}_i = n_i b_i \vec{E}. \tag{11}$$

Here n_i and kT_i are the density and temperature of the ions, $\vec{u}_i$ is the directed velocity, j_i is the ion current density, and b_i is the ion mobility.

The current densities of ions (11) and electrons (9) are combined into discharge total current density

$$\vec{j}_0 = \vec{j}_i + \vec{j}_e; \quad \frac{1}{r}\frac{d}{dr} r j_0(r) = 0,$$

which is related to the discharge current i in magnetron geometry by

$$i = 2\pi e L r j_0(r), \tag{12}$$

where L denotes the length of magnetron discharge. It is seen from Eq. (12) that the current density $j_0(r)$ decreases from cathode to anode and is inversely proportional to the radius, providing constancy of the discharge current. The electron current density at the cathode is small and constitutes the fraction γ from the ion one $j_e(R_C) = \gamma j_i(R_C)$. At the anode the total current is transported by the electrons $j_e(R_A) = j_0(R_A)$.

By supplementing Eqs. (10), (11) with Poisson's equation

$$div \vec{E} = 4\pi e(n_i - n_e)$$

and taking their projections on the positive direction of the r axis, we obtain the following closed system of equations for self-consistent determination of discharge parameters:

$$\frac{1}{r}\frac{d}{dr} r j_i(r) = -[I_d(r) + I_s(r)], \tag{13}$$

$$n_i(r) = j_i(r)/[b_i(E)E], \tag{14}$$

$$\frac{1}{r}\frac{d}{dr} rE = -4\pi e(n_i - n_e). \tag{15}$$

In the system (13)–(15) the field E and ion current density j_i are the positive values.

The solution of the self-consistent problem has been performed in the following way. Some initial field profile was given to define the radial course of the potential. The kinetic equation was solved for this potential profile, the distribution function obtained and the rates of ionization processes, and particle and current densities were calculated simultaneously with the calculation of the distribution function. Then the fulfillment of particle and energy balances was checked. The calculated EDF was normalized at the value of discharge current density at the anode, as long as the density of electron current coincided with that of the total current at the anode. The normalization coefficient obtained from this normalization condition for the EDF was then used to recalculate the relevant macroscopic parameters into absolute units. The self-consistent electric field was found by establishing technique employing integration of the system (13)–(15) in the direction from anode to cathode and by the approximation of the curve $E(r)$ obtained on each iteration with high order polynomial. The calculations of the EDF and macroscopic properties were repeated for every new dependence of $E(r)$ obtained at the end of each iteration.

RESULTS AND DISCUSSIONS

The results of the self-consistent solution refer to discharge in argon at pressure $p = 0.02$ Torr, magnetic field strength $B = 200$ G, discharge current $i = 72$ mA, radii of cathode and anode $R_C = 0.5$ cm and $R_A = 3$ cm, and length of magnetron discharge $L = 12$ cm. The ionization processes were treated with the coefficient of energy redistribution $\beta = 0.25$. The value for ion mobility and its dependence on electric field strength was taken in the form $b_i(E) = b_{i0}[1 + \alpha(E/p)]^{-1/2}$, $b_{i0} = 1460$ cm^2 V^{-1} s^{-1}, $\alpha = 0.0264$ for Ar at 1 Torr [21].

On the whole, the fall of the potential (Fig. 2) is concentrated in the cathode region attaining the magnitude of about 250 V, which exceeds those in the positive column and anode region. These results appear to be very expected as long as electron ''mobility'' exceeds that of the ions at not too large magnetic fields. In strong magnetic fields of the order of thousands of Gauss, the electron mobility is considerably reduced and becomes comparable to ion mobility, which leads to an increase in the anode fall and the consequent decrease of the cathode fall.

The electric field strength (Fig. 3) attains 2200 V/cm at the cathode and then abruptly drops towards the end of the cathode sheath. In the negative glow region the profile of the electric field has a minimum, with minimal field value 4 V/cm attained at the point $r = 0.9$ cm. In the positive column the electric field strength increases towards the anode initially slowly, and faster afterwards.

The electron distribution function (Fig. 4) that is formed in similar fields has the following peculiarities. The EDFs in the cathode region are actually the distribution functions of high-energy electrons. The fraction of slow electrons contributing to particle density is very small, and the EDF's ''tail'' contains electrons with a continuous energy spectrum extending up to 200–250 eV. This is caused by quick acceleration due to a large difference between the potentials in the

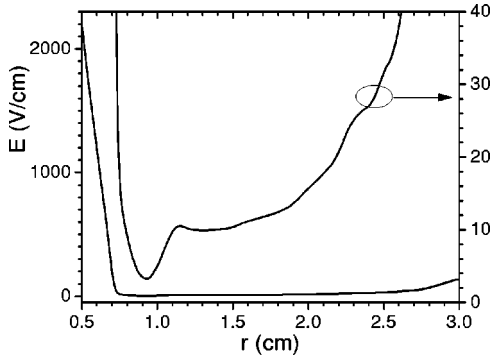

FIG. 3. Radial profile of the electric field in full discharge (left scale) and the field's details in the bulk plasma (right scale), obtained as a result of the self-consistent solution.

cathode sheath of both the cathode ejected electrons and the slow electrons that appears in exciting and ionizing collisions. In the transitional region between the cathode sheath and negative glow region, electrons come to the region of small field. Backscattered slow electrons are weakly heated by this field and their density increases quickly. Thus, in the negative glow region a peak of slow electrons is formed in the EDF. In the positive column the fast electrons lose their energy to atom excitation and ionization, which leads to a gradual decrease of the EDF scale in the inelastic region, whereas the decrease in the number of slow electrons follows from an increase in electric field strength under almost constant electron current density. The EDF formation in the anode region is governed by the action of two factors. First, due to the presence of the anode which is the electron absorbing surface, the EDF is additionally depleted in slow electrons. These slow electrons are affected by the anode starting from quite large distances from the anode surface, of the order of the energy relaxation length $\lambda_\varepsilon \sim U_{\mathrm{ex}}/eE$

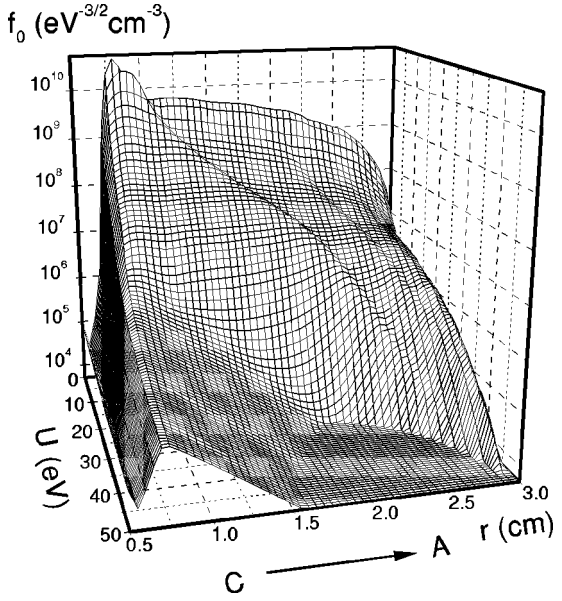

FIG. 4. Electron distribution function in magnetron discharge, as obtained by the self-consistent solution for the electric field shown in Fig. 3.

~ 0.4 cm. Second, in the anode region the EDF becomes additionally populated in fast electrons, which is caused by their acceleration due to the strong field in the anode-fall region. These fast electrons sink on the anode starting at much smaller distances than the slow ones, resulting in the formation of the EDFs populated in high-energy electrons which cause additional ionization in the anode-fall sheath.

The supplementary wavelike structure seen in the EDF (Fig. 4) is stipulated by the phenomena of electron relaxation in inhomogeneous fields as discussed in detail, particularly in Ref. [1–4]. Specifically, Ref. [1] has demonstrated the origin of a wave in the electron distribution function when electrons pass through a spatially limited region where electric field strength is smaller than that in the neighboring regions. The origin of these oscillations is connected with an overpopulation of slow electrons in the region of a weak field, whose subsequent acceleration by a stronger field is reflected in the appearance of the local maximum in the EDF, which moves towards the anode almost along the line of the $\varepsilon = \mathrm{const}$. Backscattering of these electrons in inelastic collisions leads to the formation of subsequent local maxima in the distribution function and the observed wavelike structure.

The excitation and ionization rates, particle and current densities, and electron average energy are represented in Fig. 5. The rates of excitation and total ionization [Fig. 5(a)] are maximal approximately at the boundary of cathode-fall and negative glow regions. Near the anode these rates provided by fast electrons increase, unlike the behavior of the stepwise ionization rate, which is determined by slow electrons.

The distribution of ionization sources stipulates the radial course of electron j_e and ion j_i current densities combining into total current density j_0 [Fig. 5(b)]. The decrease of discharge current density with radial position is caused by discharge geometry. It is seen from the figure that in the regions of cathode fall and negative glow the current is transported by the ions, and by the electrons in the positive column and the anode region. The self-consistent solution of the problem gives the value of $\gamma \approx 0.1$ for the electron secondary emission coefficient, which agrees well with the values used in similar problems on cathode phenomena [22].

The radial distributions of charged particle densities [Fig. 5(c)] generally reflect the EDF behavior at small energies. However, the wavelike structure seen in the EDF, does not itself appear in radial dependencies of electron density. The density distributions indicate that plasma is generally quasineutral, the positive space-charge sheath is formed in the cathode region, and a small negative space-charge sheath can be seen near the anode. The particle densities attain their maximal values of about 4×10^{10} cm^{-3} in the region of the field minimum and then decrease towards the anode. The average electron energy [Fig. 5(d)] reveals nonmonotonic radial dependence equal to approximately 4 eV in the positive column and attaining considerably larger values in the near-electrode regions.

It is interesting to consider the electron relaxation process in the cathode sheath. Since electrons emitted from the cathode have an energy spectrum within a few eV, a sufficiently narrow energy distribution function of electrons whose energies do not exceed the excitation threshold can be taken at

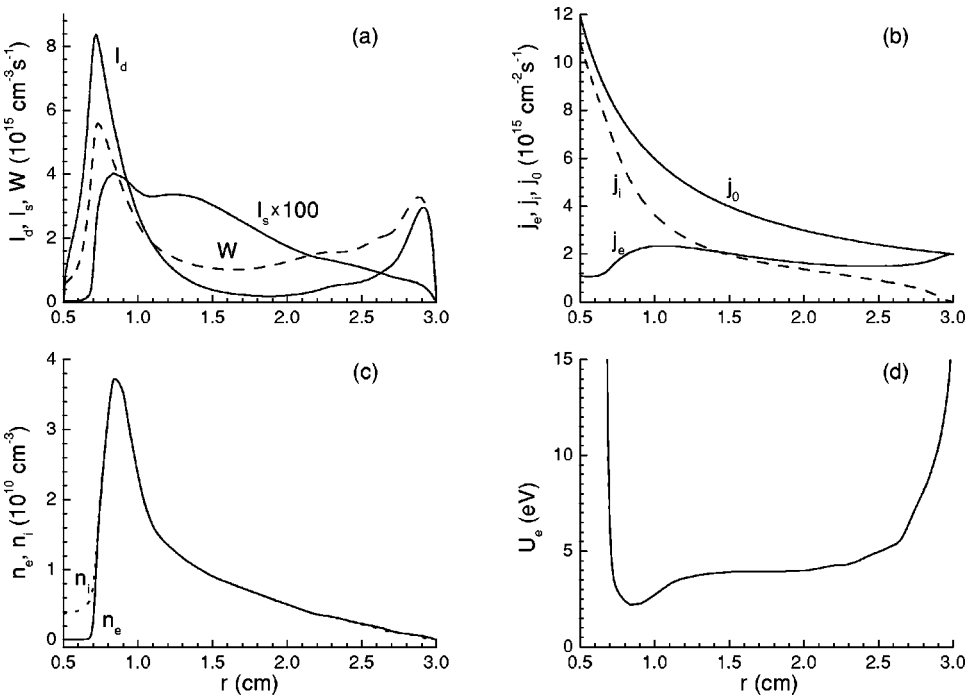

FIG. 5. Radial profiles of excitation and ionization rates (a), particle (b), and current (c) densities, and electron average energy (d) in magnetron discharge.

the cathode as the initial one. The examples of relaxation of such distribution in the self-consistent field (Fig. 3) are represented in Fig. 6(a) for the coefficient $\beta=0.25$ and in Fig. 6(b) for $\beta=0.1$. As long as the cathode sheath is small and the electric field in the sheath decreases linearly, the relaxation pattern has an appearance similar to that obtained in Ref. [17] for cylindrical discharge. Electrons of the initial distribution are accelerated by the cathode-fall field and make up a beam whose position in energy space corresponds to the potential energy gained by these electrons up to that space position. When the kinetic energies of the electrons belonging to an initial EDF attain the excitation threshold, the electrons can excite atoms. Backscattering processes lead to the formation of a second group of electrons in the EDF at energies smaller than those of the excited electrons at the excitation threshold. These two groups of electrons, clearly seen in Fig. 6, are accelerated by the field and lose energy during exciting and ionizing collisions. In the case of a broad initial distribution function, the resultant EDFs have a smooth energy dependence and reveal no similar peaks. Formation of the additional maxima in the EDF, which are distributed over an energy range much farther from the beam-like electrons, is caused by the appearance of slow electrons in the ionization processes. It is seen that these maxima at $\beta=0.25$ [Fig. 6(a)] are separated from each other by larger energies than they are in the case with $\beta=0.1$ [Fig. 6(b)]. This fact is easily understood if one considers the energies attained in the ionization event by the two outgoing electrons in both cases. If the quantity β had a continuous range of values, these additional maxima, stipulated by ionization collisions, would disappear.

It should be noted that the solution of the self-consistent problem is influenced very little by the form of the initial distribution at the cathode and depends weakly on the coefficient of energy redistribution between slow electrons β when it falls within the range $0.1<\beta<0.5$. To find a solution with the same order of accuracy for smaller β values, considerably more computational work is required.

When comparing the results of this modeling with those of [5], one can observe the qualitative agreement in radial distributions of the parameters. The EDFs in both models

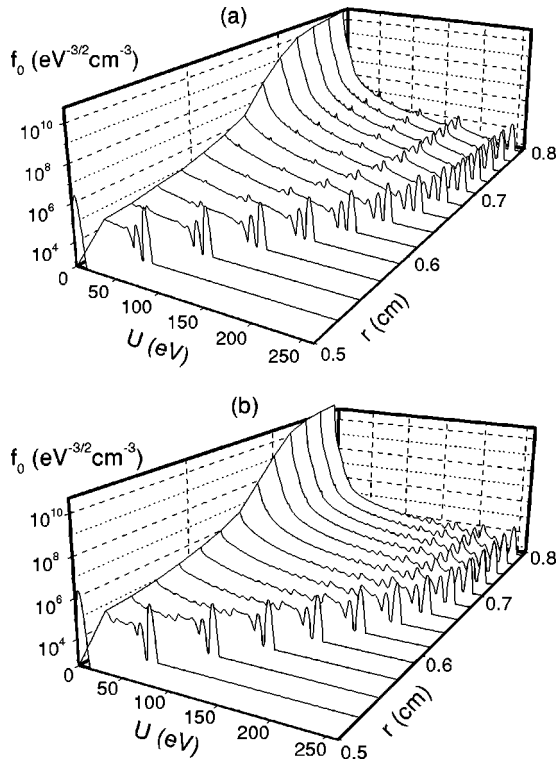

FIG. 6. Relaxation patterns of the electron distribution functions in the cathode sheath for two values of energy redistribution coefficient in ionization event (a) $\beta=0.25$ and (b) $\beta=0.1$.

have similar variation with radial position. Some quantitative distinctions are noticeable in the absolute values of the electron average energy and the fall of the potential between cathode and anode. At the same time, the kinetic model is unable to interpret oscillations of the electric field strength and particle density appearing in PIC results in the anode region.

CONCLUSION

The kinetic model of magnetron configuration discharge in crossed electric and magnetic fields developed in the present paper permitted us to perform the uniform description of plasma over the discharge gap and obtain self-consistently the distributions of internal plasma quantities from cathode to anode. The electron component has been considered based on the numerical solution of the spatially inhomogeneous kinetic equation by a two-term approximation, whereas the development of an appropriate numerical scheme for the solution was required to correctly take into account the ionization processes. To find the self-consistent solution, the kinetic equation has been supplemented by equations describing the ion motion in the collisional regime and Poisson's equation. The results obtained for the field profile, distribution function, and macroscopic properties describe the formation of the cathode-fall and negative glow regions, the extended positive column and the anode sheath.

The development of a similar model for discharge at low pressures and weak magnetic fields became possible due to two factors. First, the presence of the magnetic field abruptly decreases the distribution function anisotropy in the radial direction and second, codirection of the fields of current transport and ambipolar diffusion, stipulated by the discharge geometry, reduces the problem into one dimension in coordinate space.

ACKNOWLEDGMENTS

This work was financially supported by the Deutsch Forschungsgemeinschaft (DFG) in the framework of the Sonderforschungsbereich SFB 198 Greifswald ''Kinetics of partially ionized plasma,'' by Grant No. GACR 202/00/1689, and by the Laboratoire de Physique des Gaz et Plasmas of the Université Paris–Sud.

APPENDIX: NUMERICAL SOLUTION

As the initial boundary value problem is solved for a parabolic partial differential equation with evolution coordinate ε, the calculations of the EDF as a function of radius are required at every step in total energy. When constructing the numerical scheme for solving the kinetic equation (7), it is necessary to take into account the presence of large gradients of the electric field, and to store resultant EDFs for accurate treatment of ionizing collisions. Taking these factors into account, the kinetic equation has been discretized on the mesh, equidistant in total energies and nonequidistant in radial position.

In region II where $\varphi(R_a) \leqslant \varepsilon < 0$, the grid in n_{II} points was introduced according to

$$\varepsilon_i = \Delta\varepsilon \cdot i, \quad \Delta\varepsilon = \varphi(R_a)/n_{\mathrm{II}}, \quad i = -1, -2, \ldots -n_{\mathrm{II}}.$$

In region I the step in energy was taken to be the same and the number of grid points n_{I} was determined according to the value U_∞ at which the initial distribution function vanishes, i.e.,

$$n_{\mathrm{I}} = U_\infty/\Delta\varepsilon; \quad \varepsilon_i = \Delta\varepsilon \cdot i; \quad i = n_{\mathrm{I}}, n_{\mathrm{I}}-1, \ldots, 0.$$

The grid points in the radial coordinate are determined thus from the condition

$$\varepsilon_i = -e\varphi(r_{-i}) \quad i = 0, -1, \ldots, -n_{\mathrm{II}}$$

and depend on the radial course of the potential.

The terms of Eq. (7) were replaced at the internal grid points (ε_i, r_j) by using finite-difference approximations in second-order accuracy. Due to the choice of the nonequidistant radial grid, the first derivatives with respect to the radius can be represented in the following form providing second-order accuracy:

$$\partial f_0(\varepsilon,r)/\partial r|_{\varepsilon_i, r_{j-1}} = \frac{1}{\Delta r_j}[-\alpha_j(f_{i,j+1} - f_{i,j}) - (2+\delta_j)(f_{i,j-1} - f_{i,j})],$$

$$\partial f_0(\varepsilon,r)/\partial r|_{\varepsilon_i, r_j,} = \frac{1}{\Delta r_j}[\alpha_j(f_{i,j+1} - f_{i,j}) - \delta_j(f_{i,j-1} - f_{i,j})],$$

$$\partial f_0(\varepsilon,r)/\partial r|_{\varepsilon_i, r_{j+1}} = \frac{1}{\Delta r_j}[(2+\alpha_j)(f_{i,j+1} - f_{i,j}) + \delta_j(f_{i,j-1} - f_{i,j})],$$

where $f_{i,j}$ denotes $f_0(\varepsilon_i, r_j)$ and

$$\Delta r_j = r_{j+1} - r_{j-1}, \quad \alpha_j = \frac{r_j - r_{j-1}}{r_{j+1} - r_j}, \quad \delta_j = 1/\alpha_j.$$

The second derivative with respect to r, which includes radially dependent coefficients, can be written as

$$\left.\frac{\partial}{\partial r}\left(A(\varepsilon,r)\frac{\partial f_0(\varepsilon,r)}{\partial r}\right)\right|_{\varepsilon_i, r_j} \approx \frac{1}{\Delta r_j}[\alpha_j(A_{i,j+1}\partial f_0/\partial r|_{i,j+1} - A_{i,j}\partial f_0/\partial r|_{i,j}) - \delta_j(A_{i,j-1}\partial f_0/\partial r|_{i,j-1} - A_{i,j}\partial f_0/\partial r|_{i,j})],$$

where $A_{i,j}$ denotes kinetic coefficient taken at the point (ε_i, r_j).

The appearance of slow electrons in exciting and ionizing collisions $(D_{i,j})$ is described by the distribution function at the shifted energy of $\varepsilon_i + U_{\mathrm{sh}}$ which usually does not fit mesh

points. The distribution function $f_0(\varepsilon_i + U_{\mathrm{sh}}, r_j)$ was represented on the same energy mesh by a parabolic interpolation through the corresponding mesh points. The tridiagonal linear equation system obtained at every fixed total energy was supplemented by boundary conditions discretized in a similar way on the same mesh.

[1] F. Sigeneger and R. Winkler, Contrib. Plasma Phys. **36**, 551 (1996).

[2] F. Sigeneger and R. Winkler, Plasma Chem. Plasma Process. **17**, 1 (1997).

[3] F. Sigeneger, Yu.B. Golubovskii, I.A. Porokhova, and R. Winkler, Plasma Chem. Plasma Process. **18**, 153 (1998).

[4] Yu.B. Golubovskii, V.A. Maiorov, I.A. Porokhova, and J. Behnke, J. Phys. D **32**, 1391 (1999).

[5] C. Csambal, J. Rusz, P. Kudrna, J. F. Behnke, and M. Tichy, *14th International Symposium on Plasma Chemistry, 1999, Prague, Czech Republic*, Symposium Proceedings Vol. II, edited by M. Hrabovsky, M. Konrad, and V. Kopecky (Institute of Plasma Physics, 1999), pp. 613-618.

[6] T.A. van der Straaten, N.F. Cramer, I.S. Falconer, and B.W. James, J. Phys. D **31**, 177 (1998); **31**, 191 (1998).

[7] T.M. Minea, J. Bretagne, and G. Gousset, IEEE Trans. Plasma Sci. **27**, 94 (1999).

[8] N.A. Tran, E. Marode, and P.C. Johnson, J. Phys. D **10**, 2317 (1977).

[9] J.P. Boeuf and E. Marode, J. Phys. D **15**, 2169 (1982).

[10] N. Sato and H. Tagashira, J. Phys. D **18**, 2451 (1985).

[11] J.E. Lawler, E.A. Den Hartog, and W.N.G. Hitchon, Phys. Rev. A **43**, 4427 (1991).

[12] A. Fiala, L.C. Pitchford, and J.P. Boeuf, Phys. Rev. E **49**, 5607 (1994).

[13] K.G. Muller, Z. Phys. **169**, 432 (1962).

[14] V.I. Kolobov and L.D. Tsendin, Phys. Rev. A **46**, 7837 (1992).

[15] M. Broglia, F. Catoni, A. Montone, and P. Zampetti, Phys. Rev. A **36**, 705 (1987).

[16] J.P. Boeuf, Appl. Phys. **63**, 1342 (1988).

[17] G. Petrov and R. Winkler, Plasma Chem. Plasma Process. **18**, 113 (1998).

[18] Yu.B. Golubovskii, S.H. al-Havat, and L.D. Tsendin, Sov. Phys. Tech. Phys. **32**, 760 (1987).

[19] I.A. Porokhova, Yu.B. Golubovskii, C. Wilke, and A. Dinklage, J. Phys. D **32**, 3025 (1999).

[20] R.E. Robson, Aust. J. Phys. **34**, 223 (1981).

[21] S.C. Brown, *Basic Data of Plasma Physics* (American Institute of Physics, New York, 1993).

[22] Y. P. Raizer, *Gas Discharge Physics* (Springer-Verlag, Berlin, 1991).